small method
www.small-methods.com

Transient Photovoltage Measurements on Perovskite Solar Cells with Varied Defect Concentrations and Inhomogeneous Recombination Rates

Zi Shuai Wang, Firouzeh Ebadi, Brian Carlsen, Wallace C. H. Choy, and Wolfgang Tress**

In all kinds of solar cells, transient photovoltage (TPV) decay measurements have been used to determine charge carrier lifetimes and to quantify recombination processes and orders. However, in particular, for thin-film devices with a high capacitance, the time constants observed in common TPV measurements do not describe recombination dynamics but *RC* (*R*: resistance, *C*: capacitance) times for charging the electrodes. This issue has been revisited for organic and perovskite solar cells in the recent literature. Here, these discussions are extended by analyzing a perovskite model system (Bi defects in $Cs_{0.1}FA_{0.9}Pb(Br_{0.1}I_{0.9})_3$ in which defect recombination can be tuned. It is found that TPV, intensity-modulated photovoltage spectroscopy, and impedance spectroscopy yield the same time constants that do not describe recombination dynamics but are limited by the differential resistance of the diode and the geometric capacitance in common light intensity ranges (<1 sun). By employing numerical device simulations, it is found that low charge carrier mobility can furthermore limit the TPV time constants. In samples with spatially nonuniform recombination dynamics, two time constants are measured, which depend on the charge carrier generation profile that can be tuned by the wavelength of the incident light. In that case, numerical simulation provides insights into recombination and charge transport processes in the device.

1. Introduction

One major loss mechanism in solar cells is non-radiative recombination. Understanding this process becomes crucial in particular for solar cells based on perovskites, as these materials provide sufficient absorption and charge carrier mobilities, resulting in light harvesting and charge carrier collection efficiencies close to unity in the relevant photon wavelength range and under short circuit conditions.[1] Therefore, understanding and controlling the recombination, which limits the obtainable photovoltage and ultimately the fill factor, is of high interest for such devices.[2] Thus, experimental methods are desirable to characterize recombination. Whereas steady-state measurements such as photoluminescence and electroluminescence spectra and yields are more straightforward to analyze,[3–5] transient optoelectronic measurements are more difficult to interpret. However, these transient measurements are desirable to quantify recombination rates that compete, for example, at maximum power point, with transport and extraction rates.[6] The typical experimental methods are transient photovoltage (TPV) decay measurements,[7–9] also combined with charge extraction,[10] and optoelectronic measurements in the frequency domain such as intensity-modulated photovoltage[11] (IMVS) and classical impedance spectroscopy[6] (EIS). Carried out as a function of the light intensity, they can yield information on the dependence of recombination on charge carrier density (reaction order).[12]

All these measurements are based on small-signal perturbations to determine a characteristic time that is supposed to describe recombination processes. Indeed, these techniques have been widely applied to organic and perovskite solar cells. However, the obtained reaction orders can be influenced by spatial inhomogeneities of charge carrier concentrations[13] and measured time constants can be limited by capacitive effects.[14,15] More precisely, the process that governs the change of the photovoltage might not be limited by recombination times but by displacement of charge, that is, the charging and discharging times of the electrodes, as this process is required to measure a change of the external voltage. This spatial redistribution of the

Z. S. Wang, F. Ebadi, B. Carlsen
Laboratory of Photomolecular Science
Institute of Chemical Sciences and Engineering
École Polytechnique Fédérale de Lausanne
Lausanne 1015, Switzerland

Z. S. Wang, Prof. W. C. H. Choy
Department of Electrical and Electronic Engineering
University of Hong Kong
Pokfulam Road, Pokfulam, Hong Kong SAR, China
E-mail: chchoy@eee.hku.hk

Dr. W. Tress
Department of Chemistry and Biochemistry
University of Munich
Munich 81377, Germany
E-mail: wolfgang.tress@lmu.de

The ORCID identification number(s) for the author(s) of this article can be found under https://doi.org/10.1002/smtd.202000290.

© 2020 The Authors. Published by WILEY-VCH Verlag GmbH & Co. KGaA, Weinheim. This is an open access article under the terms of the Creative Commons Attribution License, which permits use, distribution and reproduction in any medium, provided the original work is properly cited.

DOI: 10.1002/smtd.202000290

 © 2020 The Authors. Published by WILEY-VCH Verlag GmbH & Co. KGaA, Weinheim

photogenerated carriers cannot be neglected in ultrathin-film solar cells, and models based on simple rate equations without considering the spatial distribution of charge carrier densities are not sufficient. Undoubtedly, corrections for capacitive effects have to be included in the analysis. This issue has been discussed in the literature various times[14,16,17] and has been recently revisited by several studies comparing different thin-film technologies,[15] using thicker perovskite solar cells,[18] and looking at it from a more theoretical perspective.[19] The conclusion from these publications is that in most cases of perovskite solar cells measured under moderate light intensities, recombination dynamics cannot be captured by TPV.

In our study, we come to the same conclusion by performing a comparative experimental case study of perovskite solar cells with different defect concentrations introduced by adding small quantities of bismuth to our absorber material. We take the journey starting from experimental TPV, IMVS, and EIS data, which, interpreted as recombination times, are not consistent with the steady-state device data obtained from the current–voltage curve. Instead, we measure the charging and discharging of the electrodes, as verified by a comparison with the experimentally determined *RC* time and by investigating a thinner control device. We extend our study for inhomogeneous recombination rates and mobilities in the absorber and probe those by illumination with light of different wavelengths. Comparing the experimental data with device simulation, we shed light on the origin of a second lifetime, often observed in TPV measurements,[20–22] but so far not fully understood. It turns out that TPV on perovskite solar cells is a complex experiment that under some circumstances can provide information beyond steady-state measurements, which is, however, not straightforward to analyze.

2. Results and Discussion

The perovskite devices under investigation contain a perovskite layer with the nominal composition of $Cs_{0.1}FA_{0.9}Pb(Br_{0.1}I_{0.9})_3$ (FA stands for formamidinium) in a stack consisting of glass/fluorine-doped tin oxide (FTO)/TiO_2 (50 nm)/mesoporous TiO_2 (≈150 nm)/perovskite (≈500 nm)/doped spiro-MeOTAD (≈150 nm)/Au (80 nm). We deliberately introduce a defect by adding BiI_3 to the precursor solution as described by Yavari et al.[23] (for experimental details, see the study by Ebadi et al.[24]). **Figure 1**a shows the current density–voltage (*JV*) curves of two representative devices containing 0 (labeled Ctrl) and 0.2 at% Bi (referred to Pb). The major difference between the two curves can be found in the short-circuit current density and the open-circuit voltage (V_{oc}), which is considerably decreased upon addition of Bi (from 1.1 to 0.9 V). As the band gap of the perovskite remains unaltered, the changed V_{oc} can be directly taken as a result of an increased share of non-radiative recombination in the solar cells. Luminescence experiments both on films and devices, in steady state and transient as presented by Yavari et al.[23] confirm this interpretation. Consequently, the higher non-radiative recombination rate constants, either in the bulk or at the surface, reduce the V_{oc} of the Bi-containing device. This comes along with lower charge carrier densities at a given light intensity, that is, charge carrier generation rate.

In equation, we can write[25]

$$eV_{oc} = E_g - kT \ln \frac{N_C N_V}{n(I,R)\,p(I,R)} \tag{1}$$

where E_g is the bandgap, k the Boltzmann constant, T the temperature, N_V and N_C are effective densities of states in valence and conduction band, respectively. The denominator contains the product of electron (n) and hole (p) density, which are a function of the light intensity I and the recombination rate R, which depends on n and p. At V_{oc}, all photogenerated charges recombine and R equals the generation rate of electron–hole pairs: $R(n) = G \propto I$. In the small signal perturbation methods, the recombination rate at a given background intensity and respective (majority) charge carrier density n_0 can be approximated by $R(n_0) = \Delta n/\tau(n_0)$, yielding $\tau(n_0)$ as an effective recombination lifetime that can be determined from a small-signal TPV experiment: $\frac{d\Delta V_{oc}(t)}{dt} \propto \frac{d\Delta n}{dt} \Rightarrow \Delta V_{oc}(t) \propto \exp\left(-\frac{t}{\tau}\right)$. The lower the τ, the faster is the overall recombination, that is, the lower n_0 for a given I.

Based on this discussion, we would expect a considerably lower TPV decay time constant for the Bi-containing device, which should be responsible for the lower n_0 and V_{oc} at a given I. However, Figure 1b shows that the low-V_{oc} device

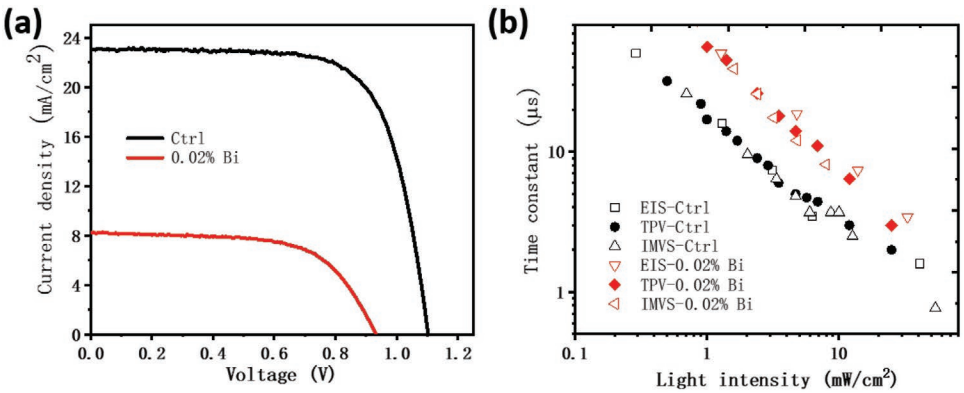

Figure 1. Characterization of solar cells with low (Ctrl) and high defect concentrations (0.02% Bi). a) *JV* curves of devices measured under simulated solar light (scan rate of –50 mV s^{-1}). b) Small signal perturbation data from TPV, IMVS, and EIS measured under white LED light.

© 2020 The Authors. Published by WILEY-VCH Verlag GmbH & Co. KGaA, Weinheim

shows comparable and even slightly higher time constants (τ) in the overall intensity range investigated. This result is independent of the measurement technique used to obtain τ. The technique corresponding to TPV in the frequency domain, IMVS, where the illumination is sinusoidally modulated and the voltage response measured, delivers the same results. Also using an electrical stimulus in EIS (sinusoidal small-signal perturbation voltage applied) under illumination and open circuit results in the same τ, when obtained from the intermediate spectral range. This coincidence has also been reported for organic solar cells.[26] Therefore, we can hypothesize that these measurement techniques characterize the same process, although EIS is different to the other techniques. EIS measures the current with a low-input resistance instead of the open-circuit voltage response. For a direct comparison of τ of the two devices we might want to compare τ at the same n_0, because τ might depend on n_0 as is the case for any nonlinear ("higher-order") recombination process. Such plots of τ versus n_0 are commonly discussed, where n_0 is obtained from charge extraction measurements.[9,12,18] To avoid the difficulties of this measurement, we can use V_{oc} itself because for an unmodified band gap and density of states (and constant T), V_{oc} (Equation (1)) is a unique function of the charge carrier density (if it makes sense to define a homogeneous charge carrier density). Replotted versus V_{oc} (**Figure 2**a), the trend of τ is indeed inverted, which might be taken as an indication that the recombination dynamics is indeed faster for the low-V_{oc} device. However, the strong dependence of τ on V_{oc} and light intensity with a power law of an exponent close to –1 remains unexplained. In the recombination processes discussed for perovskite solar cells, we would expect a constant lifetime in a simple Shockley–Read–Hall (SRH) model and in the case of surface recombination. A second-order process, such as radiative recombination between photogenerated charges ($R = \beta np = \beta n^2$), should yield an exponent of $-\frac{1}{2}$ as n_0 would scale with $\sqrt{I}$. In general, if τ represents a measure for recombination times at a given light intensity, a faster recombination and lower V_{oc} have to be accompanied by a reduced τ at this light intensity, independent of the resulting n_0. (A lower n_0 must be a consequence of enhanced, i.e., higher recombination rate constants.)

To confirm the observations from Figure 1b, we measured more devices, also with other concentrations of Bi and find as a common theme that τ does not decrease with the decreased V_{oc}, but increases with Bi concentration at a given light intensity (Figure S1, Supporting Information). The roughly linear increase of τ with reduced light intensity remains (Figure 1b).

Coming back to the initial discussion of *RC* limits, we compare τ with the *RC* time obtained from the capacitance and the differential resistance of the dark *JV* curve (Figure 2b). The capacitance represents the geometric capacitance and was extracted from the high-frequency regime of impedance measurements. Exchanging the intensity axis by an axis representing a photocurrent for each device at the respective light intensity, we can compare τ_{TPV} and τ_{RC}. We observe a good coincidence showing that the light-intensity-dependent τ_{TPV} does not contain more information than can already be deduced from the steady-state dark *JV* curve when knowing the geometric capacitance. This directly explains why TPV and EIS time constants coincide as both measure the *RC* response of the device. We confirm this effect by a device with a thinner perovskite layer, where we observe higher τ due to the increased capacitance ($\propto$ 1/thickness), which completely rules out that the τ we are measuring has anything to do with recombination dynamics. This explanation is not surprising given the recently reported results and discussions elaborated in the introduction.[15,18] This *RC* approach has also been formulated earlier for other solar cells and *R* is commonly approximated by the differential resistance of the diode curve.[14,27] As the *RC* time is decreasing with increasing voltage, criteria for the minimum light intensity can be formulated, under which recombination times could be seen.[19]

Using a custom-made numerical device simulator, we performed TPV simulations following the approach of the mirror-device introduced by Calado et al.[28] We extracted τ as a function of light intensity shown in **Figure 3**a, and compared simulation with experimental values. For simplification, uniform input parameters, including charge carrier generation rate, SRH recombination lifetimes, radiative recombination rate constant, and mobilities were set in the absorber, which includes both meso-TiO_2 and perovskite layer. (Details on the numerical device simulations can be found in Supporting Information.) Based on our previous work,[23] we expect that the Bi impurity only affects the SRH recombination time constant (τ_{SRH}) and possibly slightly the charge carrier mobility. Decreasing the

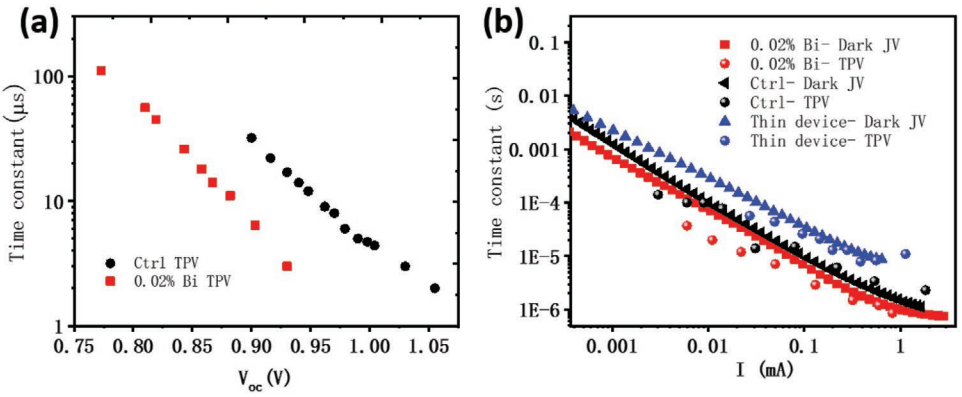

Figure 2. Transient photovoltage and *RC* limitations. a) TPV time constant plotted versus open-circuit voltage. b) Dominant TPV time constants versus photocurrent and the *RC* time constant extracted from the dark *JV* curve and geometric capacitance versus current.

© 2020 The Authors. Published by WILEY-VCH Verlag GmbH & Co. KGaA, Weinheim

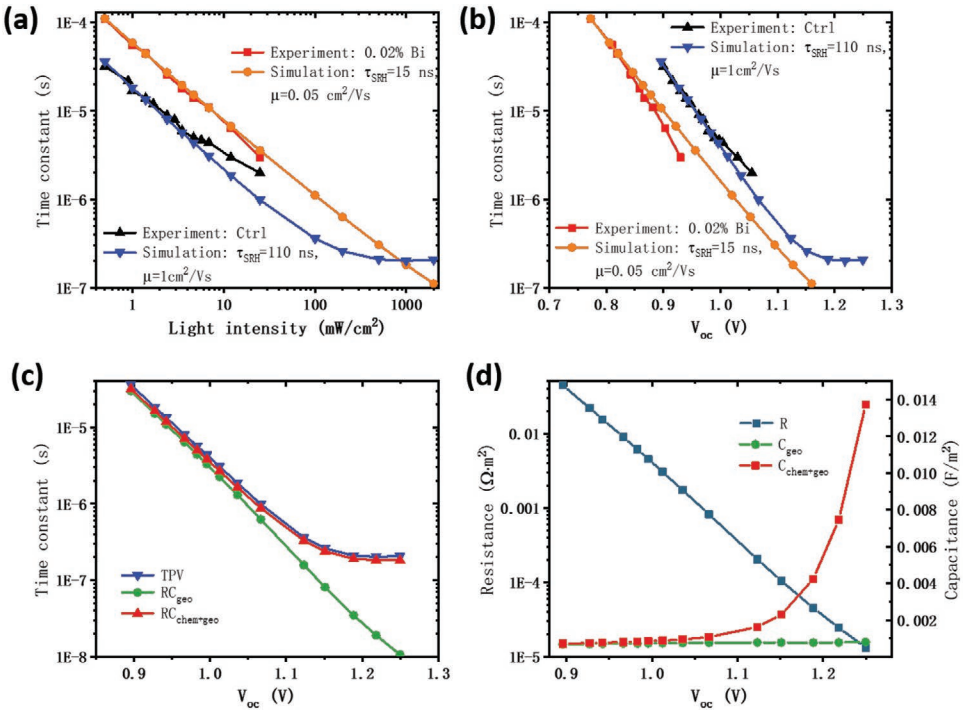

Figure 3. TPV in simulation. Simulated τ_{TPV} a) versus light intensity and b) versus V_{oc} compared with experimental data. c) Simulated τ_{TPV} compared with simulated *RC* time constants. d) Simulated resistance and capacitance (chemical and geometric) versus voltage. *R* and *C* are extracted from EIS simulations.

τ_{SRH} by roughly one order of magnitude (from 110 to 15 ns), the simulation reproduces the light intensity dependence of V_{oc} observed in the experiment (Figure 1; Figure S2, Supporting Information). When additionally decreasing the (electron and hole) mobilities from 1 to 0.05 cm^2 V^{-1} s^{-1}, the TPV results are reproduced as well (Figure 3a,b). Interestingly, consistently with experiment, the simulation predicts a higher τ_{TPV}, when plotted versus light intensity, despite the reduced τ_{SRH}. This trend inverts for light intensities >10 suns, where τ_{TPV} saturates at a value that is twice the corresponding τ_{SRH} This value is expected, if τ_{TPV} indeed represents the recombination dynamics of such a device where SRH recombination is dominant (we set $\tau_{SRH} = \tau_n = \tau_p$, resulting in $\tau_{total} = 2\tau_{SRH}$, see Supporting Information). However, such high light intensities are experimentally harder to realize and require cooling of the sample. Therefore, commonly as well as in our case the experimental data does not extend to this regime.

To elucidate what determines τ_{TPV} for lower light intensities in the simulations, *RC* time constants were extracted from simulated EIS experiments at open circuit as a function of light intensity. Resistances are deduced from the low-frequency (1 Hz) regime of the EIS data. The geometric capacitance is extracted from the high (100 MHz) and the overall capacitance (geometric+chemical[29]) from the relatively low-frequency (0.1 MHz) regimes, respectively (Figure S3, Supporting Information). In Figure 3c, the simulated τ_{TPV} is compared with the products of resistance and geometric capacitance (named as RC_{geo}) or low-frequency capacitance (named as $RC_{chem+geo}$). As already found for experiment in Figure 2, τ_{TPV} equals RC_{geo} for lower voltages (<1 V). The resistance, which decreases exponentially with increasing voltage (Figure 3d) due to the higher concentration of charge carriers (consistent with the diode equation), dominates τ_{TPV}. However, at higher voltages, the exponential increase of the chemical capacitance (Figure 3d) due to high electron and hole densities leads to a saturation of RC_{chem}, which is consistent with the saturation value of τ_{TPV} and approximately equals $2\tau_{SRH}$ (Figure 3c). Whereas the geometric capacitance mainly represents the charging and discharging of the electrodes, the chemical capacitance includes the contribution of free carrier motion and recombination to the overall capacitance of the device. Therefore, the RC_{chem} is capable of providing information on recombination dynamics and the matching with τ_{TPV} is not astonishing. On the other hand, we can conclude that even in the regime, where recombination dominates, the information of an EIS measurement is equivalent to that of a TPV measurement.

To match the experimental results in Figure 3a,b, we had to adjust the mobility (μ) besides τ_{SRH} in the simulations. With the aid of **Figure 4**, we now investigate the effect of τ_{SRH} and μ separately. When plotting τ_{TPV} versus light intensity or V_{oc} for varied τ_{SRH} at fixed μ (1 cm^2 V^{-1} s^{-1}), one can observe three regimes (Figure 4a,b): First, the power–law behavior with an exponent of –1 at lower light intensities, where τ_{TPV} at the same light intensity becomes independent of τ_{SRH} (intensity <1 mW cm^{-2} in Figure 4a). When plotted versus V_{oc} (Figure 4b), the τ_{TPV} curves shift horizontally due to the decrease of V_{oc} with lower τ_{SRH}, which is accompanied by a lower resistance of the dark *JV* curve at a selected voltage. In the second regime, clearly pronounced in the cases of very fast SRH recombination, τ_{TPV} saturates at higher voltages at around $2\tau_{SRH}$, as mentioned previously. However, in the cases of slow SRH recombination, τ_{TPV} reaches a plateau at $2\tau_{SRH}$, but continues to decrease and

© 2020 The Authors. Published by WILEY-VCH Verlag GmbH & Co. KGaA, Weinheim

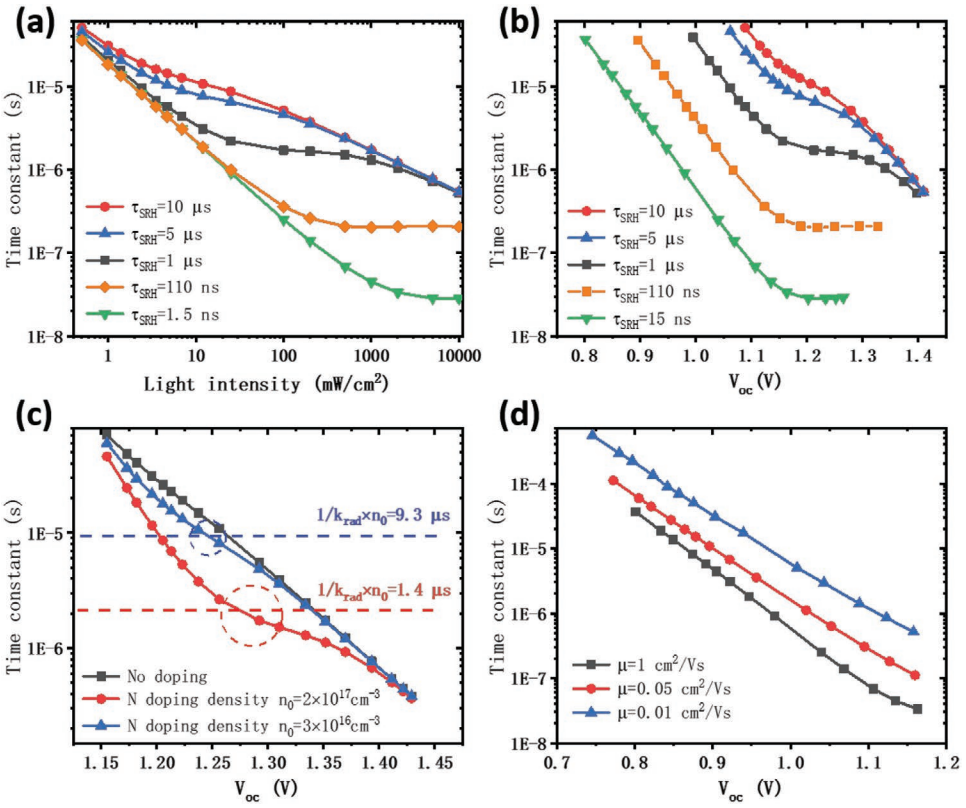

Figure 4. Dependence of TPV time constant on material parameters in simulation. Simulated τ_{TPV} versus a) light intensity and b) V_{oc} for perovskite solar cells with different recombination lifetimes. c) Simulated τ_{TPV} versus V_{oc} in the case of radiative recombination only but varied doping density. d) Simulated τ_{TPV} versus V_{oc} in perovskite solar cells with different carrier mobilities and fixed $\tau_{SRH} = 15$ ns.

converge at higher voltages, giving rise to the third regime. This convergence results from the radiative recombination, which causes a constant slope (power law with exponent of $-\frac{1}{2}$ in Figure 4a), and dominates when the charge carrier density is sufficiently high that $\beta_{rad}n^2$ rules recombination, as reported by Sandberg et al.[19] A similar behavior with a plateau can be observed in case of radiative recombination only, when considering doping of the absorber layer. The high background charge density yields a constant (minority carrier) lifetime in a certain intensity range, which causes the same feature as SRH recombination (Figure 4c). These simulation results indicate that τ_{TPV} results are not easy to interpret, even when analyzing τ_{TPV} at high light intensities.

Coming back to the first regime, we investigate the role of μ in the absorber. Figure 4d shows that a slower charge carrier transport in the perovskite layer (mobility decreased from 1 to 0.01 cm^2 V^{-1} s^{-1}) leads to an increase of τ_{TPV}, due to the higher resistance induced by the low mobilities. Lowering mobility also slightly decreases the slopes of the τ_{TPV}–V_{oc} curves, as a result of constant slopes of τ_{TPV} versus light intensity curves and increasing ideality factors (Figure S4, Supporting Information). The influence of carrier transport on τ_{TPV} can be explained by comparing the diffusion length with the thickness of the perovskite layer. Due to the uniform recombination rate constants and charge carrier mobility set in the simulation, the diffusion length simply equals $\sqrt{D\tau}$, where $D = \mu k_B T/e$ refers to the diffusion coefficient, and τ is τ_{SRH}, which is fixed as 15 ns in this case. In Figure S5a, Supporting Information, τ_{TPV} is plotted as a function of diffusion length (by varied mobility) for different perovskite layer thicknesses of 300, 500, and 700 nm. The V_{oc} in these TPV simulations only slightly varies and thus does not affect the discussion (Figure S5b, Supporting Information). A higher diffusion length leads to a decrease of τ_{TPV} until the diffusion length is comparable to the thickness of the perovskite layer, where τ_{TPV} becomes independent of the diffusion length. In the regime where the diffusion length is larger than the perovskite thickness, which means most of the free carriers can diffuse to the contacts within their lifetimes, the τ_{TPV} is only determined by the RC time constant given by recombination and geometric capacitance. These results suggest that τ_{TPV} can depend on μ in low-mobility materials. Therefore, a comparison of τ_{TPV} of different devices might not necessarily reflect a trend in recombination.[30]

We want to note that in the common extension of the diode model with the series resistance, describing additional resistive voltage losses, the series resistance does not influence τ_{TPV} as it is not involved in charging the electrodes. (This can easily be verified by connecting an external series resistance.) However, our results show that resistances that occur in the device, for example, in the perovskite layer, affect τ_{TPV}.

So far we assumed that properties of the layers are uniform. Now, we want to address cases with vertical inhomogeneities in recombination rates. We want to probe them by using

© 2020 The Authors. Published by WILEY-VCH Verlag GmbH & Co. KGaA, Weinheim

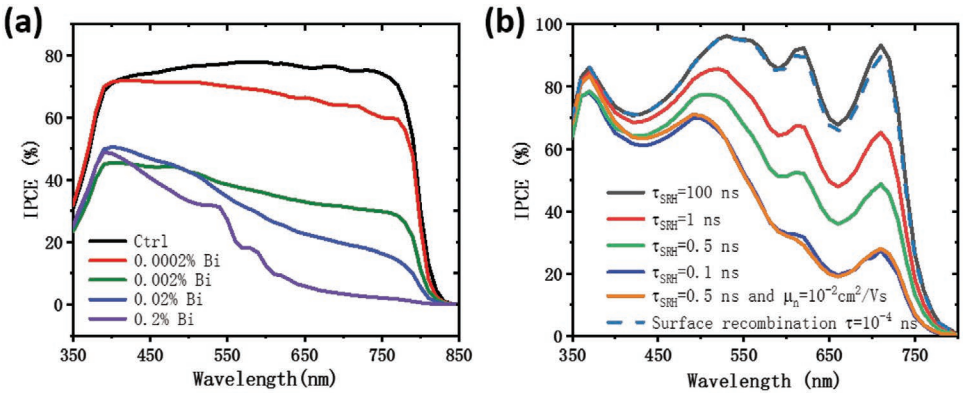

Figure 5. Incident photon to current efficiency (IPCE) for devices with different Bi contents a) measured b) simulated comparing the effect of surface recombination at the HTM, an enhanced recombination in the bulk of the perovskite, and decreased mobilities.

illumination with different wavelength to modify the charge carrier generation profile.

As recombination does not only affect V_{oc} but also the short-circuit current density (J_{sc}) (Figure 1a and the study by Yavari et al.[23]), we measured the spectral response at short circuit. The resulting incident photon to current efficiency (IPCE) in **Figure 5**a shows an overall drop with increasing Bi concentration. However, more importantly, the decrease is much more pronounced for higher wavelength. As the absorption remains unmodified, we conclude that the internal quantum efficiency (IQE) becomes indirectly a function of the wavelength through the location where charges are photogenerated. Due to the strong dependence of the absorption coefficient on the wavelength, the red light penetrates further into the layer, whereas the blue light is already absorbed in the perovskite infiltrated in the mesoporous TiO_2 layer. Therefore, upon addition of Bi, recombination in the perovskite layer or at the interface with the hole transport material (HTM) is much more enhanced compared to recombination in the TiO_2:perovskite layer. As the holes photogenerated close to the TiO_2 can pass through the perovskite to be harvested at the hole transport layer, we conclude that electrons in the bulk perovskite should be minorities there and face high recombination.

The maintained photocurrent in the TiO_2:perovskite despite the presence of Bi in the perovskite could be due to a fast extraction of electrons by injection into TiO_2, removing them from being available for recombination and instead contributing to photocurrent. Such a kinetic argument is valid as long as charges are extracted (e.g., under J_{sc}). Alternatively, Bi might be less incorporated into the perovskite that is formed in the mesoporous TiO_2 and therefore does not create defects in that region. The beneficial role of mesoporous TiO_2 in case of Bi addition is confirmed by a control experiment, where planar devices based on SnO_2 have been investigated. The performance of those devices is much more sensitive to the Bi concentration (PCE = 0 for a Bi concentration of 0.02%).

To judge whether the recombination caused by Bi is more a surface recombination or a bulk recombination in the perovskite layer, we employed our numerical device model. We separate the absorber in two layers, one of 100 nm thickness representing the TiO_2:perovskite and one (400 nm) the bulk perovskite. Absorptivity of the solar cell and the carrier generation rate $G(x)$ in the absorber were calculated by solving Maxwell's equations using our optical model (2D finite-difference method based, details in the study by Sha et al.[31]) with optical constants from Werner et al.[32] $G(x)$ was calculated for each wavelength (λ) and introduced into the drift-diffusion model to obtain $J_{sc}(\lambda)$. The internal quantum efficiency (IQE) of each wavelength was calculated as the ratio of the corresponding $J_{sc}(\lambda)$ to the maximum photocurrent $\left(J_{ph}(\lambda)=e\int_0^L G(x,\lambda)\,dx\right)$, where L is the thickness of the perovskite absorber. The IPCE was obtained as the product of the IQE and absorptivity. The carrier generation profile under white light and the absorptivity can be found in the Supporting Information (Figures S6 and S7, Supporting Information). The simulation results in Figure 5b indicate that the IPCE can be reproduced by introducing fast recombination in the bulk region, or slow transport (low μ) in this region, or both, but not surface recombination at the HTM interface. (Interference fringes are much more pronounced in the simulation as the scattering effect of the FTO/mesoporous TiO_2 substrate is not considered in the model.) We also simulate the light JV curves with different input parameters (Figure S8, Supporting Information) to compare with the measured JV curves in Figure 1a for consistency. The JV curves confirm that surface recombination at the HTM side mainly reduces V_{oc} but only slightly influences J_{sc}, whereas fast bulk recombination and slow electron mobility reproduce the trends in the measured JV curves. Too low hole mobility can be ruled out as the corresponding simulated fill factor is too low compared to the experiments. Therefore, from simulation, we suggest that adding Bi increases bulk recombination and reduces electron mobility in the bulk region, confirming the above descriptions and those in our previous work.[23]

In the following, we want to evaluate whether we can probe this difference in recombination also at V_{oc} using illumination of different wavelength for the TPV experiment. **Figure 6**a shows that τ_{TPV} plotted versus V_{oc} is independent of the illumination color for the device without Bi, consistent with the overall high IPCE at J_{sc}. On the contrary, τ_{TPV} of the Bi containing device depends on the illumination color and decreases when going from blue (470 nm) through white to red (620 nm) (Figure 6b). At first glance, this looks consistent with the IPCE showing higher recombination in the layer more distant from the TiO_2. On the other hand, we have been discussing with

© 2020 The Authors. Published by WILEY-VCH Verlag GmbH & Co. KGaA, Weinheim

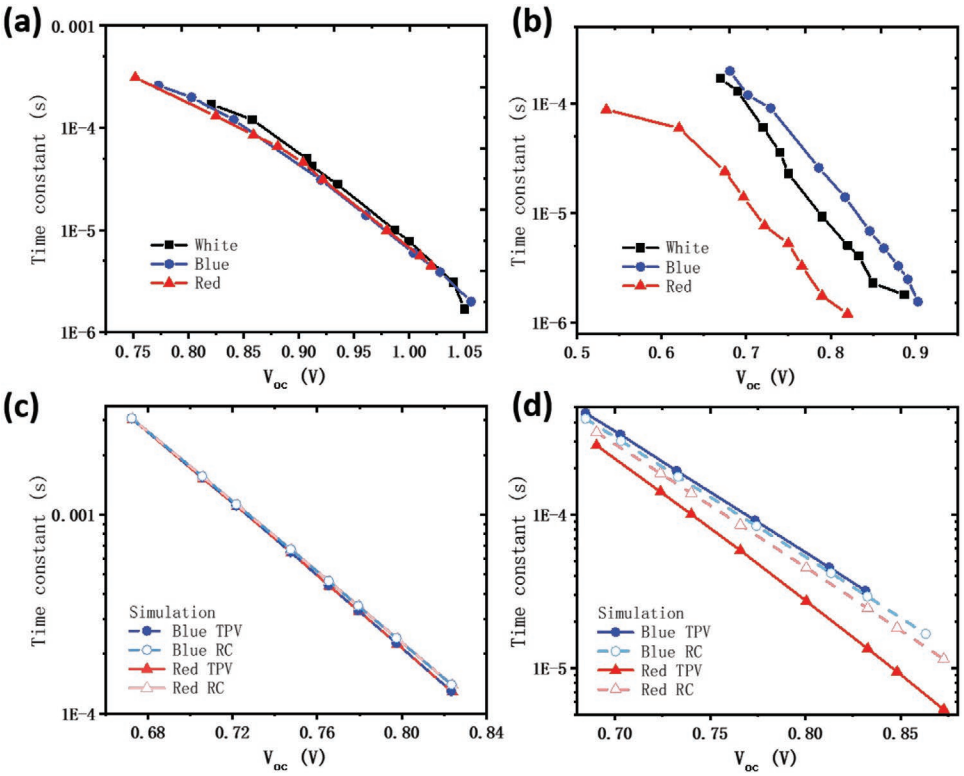

Figure 6. Colorful transient photovoltage in experiment and simulation. a,b) τ_{TPV} measured with LED light of white, blue (470 nm), and red (620 nm) color for a) Ctrl and b) 0.02% Bi devices. c,d) τ_{TPV} simulated with simplified red and blue light generation profiles in c) control and d) in device with increased recombination and reduced electron mobility in the bulk perovskite part.

the help of Figure 2b that τ_{TPV} is given by the *RC* time for charging the electrodes in this intensity range. Obviously, the simple *RC* approximation obtained from the dark case cannot explain this difference with the illumination color. However, one might argue that the *RC* time depends on voltage and illumination conditions. This is because of photoconductivity effects or voltage-dependent space charge layer width or free charge carrier densities contributing to the capacitance. However, deducing the resistance under each illumination condition did not yield strongly changed *RC* times that could explain the differences seen in Figure 6b (more details in discussions of **Figure 7**).

Hence, we revert to our simulations. Simplified generation profiles were used to represent the experiments under blue and red light (Figure S9, Supporting Information). For blue light, carrier generation is assumed in the 100 nm thick layer representing the meso-TiO_2:perovskite region, while red light is represented by a uniform generation in the adjacent 400 nm layer, representing the bulk perovskite layer. With fast SRH recombination (τ_{SRH} = 0.5 ns) and low electron mobility ($\mu_n = 10^{-2}$ cm^2 V^{-1} s^{-1}) only in the perovskite layer but not in the meso-TiO_2:perovskite layer, the simulation results show the same trend as in the Bi containing devices (Figure 6d), whereas for the control device (τ_{SRH} = 100 ns and $\mu_{n,p}$ = 1 cm^2 V^{-1} s^{-1}), no discrepancy appears between τ_{TPV} under red and blue light (Figure 6c). Also in the simulation the *RC* time constant obtained from long time scales, when charge carrier densities are equilibrated throughout the whole stack, does not depend on the illumination color and is closer to τ_{TPV} under blue light (Figure 6d). Therefore, we can conclude that in case of inhomogeneity in charge carrier generation and recombination, τ_{TPV} is affected beyond the influence of the *RC* time constant. The higher recombination in the bulk perovskite region leads to a reduction of τ_{TPV}. Therefore, the red light τ_{TPV} is lower, as the excess carriers generated by the red pulse concentrate in the bulk perovskite (400 nm) region with fast recombination rate, although the decrease of τ_{TPV} is very low as compared to the changes in τ_{SRH}. Differences of τ_{TPV} with illumination color can only be explained by inhomogeneous recombination rate constants. High, but uniform recombination does not show discrepancies between τ_{TPV} under red and blue light (Figure S10, Supporting Information). For consistency, we also simulated the *JV* curves under red and blue light using the same input parameters as in the TPV simulation, which match well with the experiments (Figure S11, Supporting Information).

The discussions so far have not addressed the fact that TPV transients cannot always be well-described with a single time constant but a good fit requires two values despite operating in a small-perturbation regime.[8] To investigate the origin of two τ_{TPV}, we select a device where this effect is strongly pronounced (0.2% Bi). Figure 7a shows that the two time constants τ_1 and τ_2 follow a similar trend with light intensity and color as already discussed with Figure 6. Interestingly, the ratio of the two time constants remains approximately unmodified in the intensity range investigated as already previously reported.[22] We added the *RC* values obtained from the differential resistance under

© 2020 The Authors. Published by WILEY-VCH Verlag GmbH & Co. KGaA, Weinheim

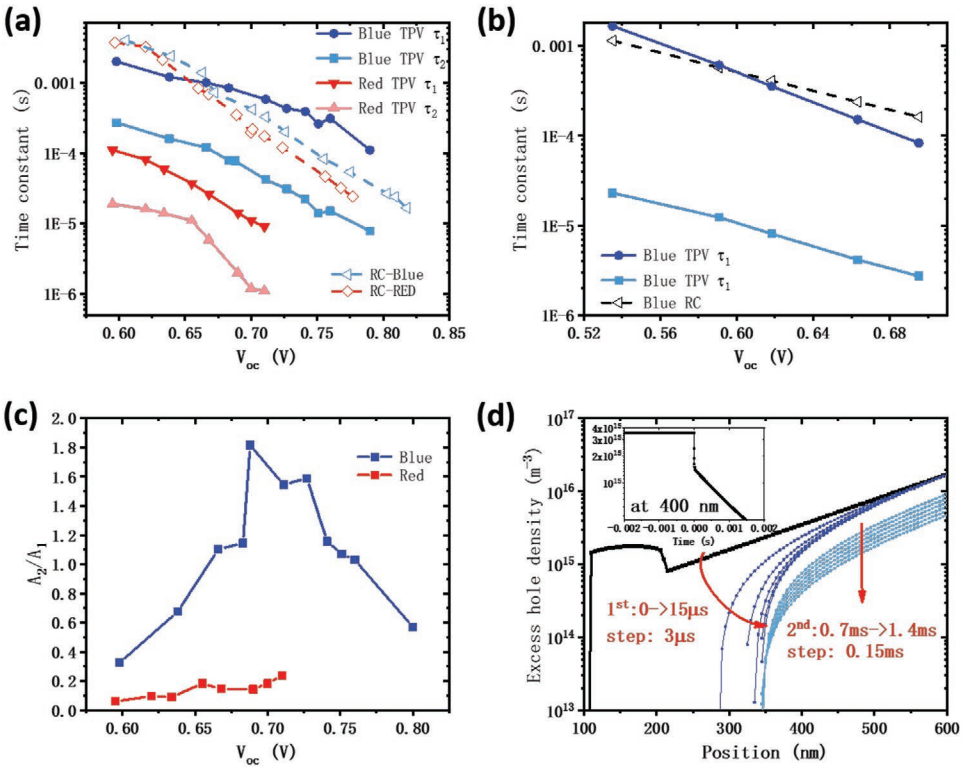

Figure 7. TPV data for 0.2% Bi device fitted with a double-exponential decay yielding two τ_{TPV}. a) Experimental data under red and blue light illumination and *RC* time constant from differential resistance at V_{oc} and geometric capacitance from EIS data. b) Simulated blue light TPV showing two τ_{TPV}. c) Ratios of the double-exponential fitting weights ($A_1\exp(-t/\tau_1) + A_2\exp(-t/\tau_2)$) of experimental blue and red light TPV. d) Simulated excess hole density evolution after light pulse in the perovskite layer; inset: excess hole density decay at 400 nm depth.

V_{oc} of the respective illumination color. Similar to the simulation in Figure 6d, these *RC* values are independent of the illumination color, and close to τ_1 of the blue light TPV. However, they cannot reproduce the red TPV data, which can be explained by the inhomogeneity of generation and recombination, as mentioned above.

Looking at the weight *A* of τ_1 and τ_2 for each color (fit function: $A_1\exp(-t/\tau_1) + A_2\exp(-t/\tau_2)$, the double exponential behavior is much more pronounced for blue illumination. Figure 7c shows the ratio of the weights A_2/A_1, and it is clear that the weights in the blue illumination case are comparable, but in the red illumination case, A_1 (the one for the higher τ_{TPV}) is almost 10 times larger than A_2; therefore, the red TPV is nearly mono-exponential, dominated by the higher τ_{TPV}. We hypothesize that a large inhomogeneity of charge carrier generation combined with nonuniform layer properties can be a reason for a pronounced multi-exponential decay. To test this in the simulation, we searched for parameter settings that could reproduce such an effect. Taking the same carrier generation profile of blue illumination applied in Figure 6d, faster SRH recombination (τ_{SRH} = 0.1 ns) and lower hole mobility (0.1 $cm^2\ V^{-1}\ s^{-1}$) in the bulk region, we were able to find a double-exponential decay of TPV in the simulation. The reason is explained with the aid of Figure 7d. As in experiment, the small-perturbation light pulse creates excess carriers in addition to the steady-state carriers. In Figure 7d, we plot the excess hole density evolution after the light pulse to unveil the two steps of the excess carrier decay. The region from 100–600 nm represents the perovskite layer including the meso-TiO_2:perovskite (100–200 nm) and the bulk (200–600 nm). Due to the carrier generation from blue light illumination concentrated in the meso-TiO_2:perovskite layer, the excess hole density in this region is higher (bold black line in Figure 7d). In the time window of tens of microseconds after removing the light pulse, fast SRH recombination occurs first in the meso-TiO_2:perovskite region as well as the part of bulk region near meso-TiO_2, because of the high local carrier density and low τ_{SRH} in the bulk. Dark blue lines show the fast change of excess hole density with a time step of 3 μs immediately after the light pulse. It can also be seen that the excess holes in the region from 100 to 400 nm will recombine within several microseconds. The fast decay is then followed by a slower process limited by the low mobility in the bulk region. Low electron mobility in the bulk region decreases the diffusion of electrons from meso-TiO_2:perovskite to the bulk, which slows down the SRH recombination rate in the bulk; in the meantime, the low hole mobility reduces the diffusion of excess holes, and forces these excess holes to recombine locally in the bulk with a slower velocity. Light blue lines show the slow change of excess hole density during this process, with time step of 0.15 ms. The excess hole density decay in the middle of the bulk region (at 400 nm depth) is shown in the inset of Figure 7d, and the corresponding TPV curve can be found in Figure S12, Supporting Information. Fast and slow process, happening at different locations in the device, lead the double-exponential decay of the excess carrier as well as the photovoltage, and can be referred to the two τ_{TPV}, respectively.

© 2020 The Authors. Published by WILEY-VCH Verlag GmbH & Co. KGaA, Weinheim

3. Conclusion

We have investigated recombination in perovskite solar cells with different defect concentrations using TPV decay measurements and simulations. We found that TPV could not capture recombination dynamics but was limited by charging of the electrodes. Thus, TPV did not provide additional information as already available from the steady-state *JV* curve and the geometric capacitance. We furthermore investigated cases of spatially highly inhomogeneous recombination, which we probed by tuning the absorption profile using monochromatic light of different wavelengths. There, we required two time constants to properly describe the TPV signal. Based on our simulations, we attributed this to recombination at different locations in the device with highly varied rate, induced by inhomogeneous generation rate and charge-carrier transport limitations. Our work further clarifies the fundamental physical meaning of the TPV time constant obtained in measurements of perovskite and other thin-film solar cells.

Supporting Information

Supporting Information is available from the Wiley Online Library or from the author.

Acknowledgements

W.T. received a funding from the European Union's Horizon 2020 research and innovation programme under the Marie Skłodowska-Curie grant agreement number 795079, hosted by Prof. Thomas Bein at Munich University, who is kindly acknowledged. Furthermore, W.T. acknowledges funding by the Swiss National Science Foundation (Ambizione Energy grant number 173617), kindly hosted by Prof. Anders Hagfeldt at EPFL. W.C.H.C. and Z.S.W. acknowledge the support of General Research Fund (grant numbers 17211916, 17204117, and 17201819) from Hong Kong Special Administrative Region, China. Z.S.W. also acknowledges funding by Swiss State Secretariat for Education, Research and Innovation (Sino Swiss Science and Technology Cooperation grant number EG-CN_03-042018), kindly hosted by Prof. Anders Hagfeldt at EPFL and the postgraduate studentship from the University of Hong Kong.

Conflict of Interest

The authors declare no conflict of interest.

Author Contributions

Z.S.W. and F.E. contributed equally to this work. Z.S.W. performed and analyzed simulations and contributed to the respective sections. F.E. fabricated devices and performed all characterization experiments and discussed the results with Z.S.W. and W.T. B.C. performed additional TPV experiments. W.C.H.C. supervised Z.S.W. and discussed the results with him. W.T. designed the study, supervised the research work, and led the writing of the article.

Keywords

drift-diffusion simulations, perovskite solar cells, recombination, transient photovoltage

Received: April 15, 2020
Revised: April 27, 2020
Published online:

[1] J.-P. Correa-Baena, M. Saliba, T. Buonassisi, M. Grätzel, A. Abate, W. Tress, A. Hagfeldt, *Science* **2017**, *358*, 739.
[2] W. Tress, *Adv. Energy Mater.* **2017**, *7*, 1602358.
[3] W. Tress, N. Marinova, O. Inganäs, M. K. Nazeeruddin, S. M. Zakeeruddin, M. Graetzel, *Adv. Energy Mater.* **2015**, *5*, 140812.
[4] D. Bi, W. Tress, M. I. Dar, P. Gao, J. Luo, C. Renevier, K. Schenk, A. Abate, F. Giordano, J.-P. C. Baena, J.-D. Decoppet, S. M. Zakeeruddin, M. K. Nazeeruddin, M. Grätzel, A. Hagfeldt, *Sci. Adv.* **2016**, *2*, e1501170.
[5] V. Sarritzu, N. Sestu, D. Marongiu, X. Chang, S. Masi, A. Rizzo, S. Colella, F. Quochi, M. Saba, A. Mura, G. Bongiovanni, *Sci. Rep.* **2017**, *7*, 44629.
[6] F. Fabregat-Santiago, J. Bisquert, G. Garcia-Belmonte, G. Boschloo, A. Hagfeldt, *Sol. Energy Mater. Sol. Cells* **2005**, *87*, 117.
[7] J. E. Mahan, T. W. Ekstedt, R. I. Frank, R. Kaplow, *IEEE Trans. Electron Devices* **1979**, *26*, 733.
[8] B. C. O'Regan, F. Lenzmann, *J. Phys. Chem. B* **2004**, *108*, 4342.
[9] T. Du, J. Kim, J. Ngiam, S. Xu, P. R. F. Barnes, J. R. Durrant, M. A. McLachlan, *Adv. Funct. Mater.* **2018**, *28*, 1801808.
[10] N. W. Duffy, L. M. Peter, R. M. G. Rajapakse, K. G. U. Wijayantha, *Electrochem. Commun.* **2000**, *2*, 658.
[11] G. Schlichthörl, S. Y. Huang, J. Sprague, A. J. Frank, *J. Phys. Chem. B* **1997**, *101*, 8141.
[12] C. G. Shuttle, B. O'Regan, M. Ballantyne, J. Nelson, D. D. C. Bradley, J. de Mello, J. R. Durrant, *Appl. Phys. Lett.* **2008**, *92*, 093311.
[13] T. Kirchartz, J. Nelson, *Phys. Rev. B* **2012**, *86*, 165201.
[14] D. Credgington, Y. Kim, J. Labram, T. D. Anthopoulos, J. R. Durrant, *J. Phys. Chem. Lett.* **2011**, *2*, 2759.
[15] D. Kiermasch, A. Baumann, M. Fischer, V. Dyakonov, K. Tvingstedt, *Energy Environ. Sci.* **2018**, *11*, 629.
[16] J. E. Mahan, D. L. Barnes, *Solid-State Electron.* **1981**, *24*, 989.
[17] L. Castaner, E. Vilamajo, J. Llaberia, J. Garrido, *J. Phys. Appl. Phys.* **1981**, *14*, 1867.
[18] D. Kiermasch, L. Gil-Escrig, A. J. Baumann, H. Bolink, V. Dyakonov, K. Tvingstedt, *J. Mater. Chem. A* **2019**, *7*, 14712.
[19] O. J. Sandberg, K. Tvingstedt, P. Meredith, A. Armin, *J. Phys. Chem. C* **2019**, *123*, 14261.
[20] N. F. Montcada, J. M. Marín-Beloqui, W. Cambarau, J. Jiménez-López, L. Cabau, K. T. Cho, M. K. Nazeeruddin, E. Palomares, *ACS Energy Lett.* **2017**, *2*, 182.
[21] L. Bertoluzzi, R. S. Sanchez, L. Liu, J.-W. Lee, E. Mas-Marza, H. Han, N.-G. Park, I. Mora-Sero, J. Bisquert, *Energy Environ. Sci.* **2015**, *8*, 910.
[22] B. C. O'Regan, P. R. F. Barnes, X. Li, C. Law, E. Palomares, J. M. Marin-Beloqui, *J. Am. Chem. Soc.* **2015**, *137*, 5087.
[23] M. Yavari, F. Ebadi, S. Meloni, Z. S. Wang, T. C.-J. Yang, S. Sun, H. Schwartz, Z. Wang, B. Niesen, J. Durantini, P. Rieder, K. Tvingstedt, T. Buonassisi, W. C. H. Choy, A. Filippetti, T. Dittrich, S. Olthof, J.-P. Correa-Baena, W. Tress, *J. Mater. Chem. A* **2019**, *7*, 23838.
[24] F. Ebadi, N. Taghavinia, R. Mohammadpour, A. Hagfeldt, W. Tress, *Nat. Commun.* **2019**, *10*, 1574.
[25] W. Tress, *Organic Solar Cells*, Springer, Berlin **2014**, p. 208.
[26] T. M. Clarke, C. Lungenschmied, J. Peet, N. Drolet, A. J. Mozer, *Adv. Energy Mater.* **2015**, *5*, 1401345.
[27] R. A. Street, *Phys. Rev. B* **2011**, *84*, 075208.
[28] P. Calado, A. M. Telford, D. Bryant, X. Li, J. Nelson, B. C. O'Regan, P. R. F. Barnes, *Nat. Commun.* **2016**, *7*, 13831.
[29] J. Bisquert, *Phys. Chem. Chem. Phys.* **2003**, *5*, 5360.
[30] M. Azzouzi, P. Calado, A. M. Telford, F. Eisner, X. Hou, T. Kirchartz, P. R. F. Barnes, J. Nelson, *Sol. RRL* **2020**, *4*, 1900581.
[31] W. E. I. Sha, W. C. H. Choy, Y. Wu, W. C. Chew, *Opt. Express* **2012**, *20*, 2572.
[32] J. Werner, G. Nogay, F. Sahli, T. C.-J. Yang, M. Bräuninger, G. Christmann, A. Walter, B. A. Kamino, P. Fiala, P. Löper, S. Nicolay, Q. Jeangros, B. Niesen, C. Ballif, *ACS Energy Lett.* **2018**, *3*, 742.

© 2020 The Authors. Published by WILEY-VCH Verlag GmbH & Co. KGaA, Weinheim